



Trans. Nonferrous Met. Soc. China 34(2024) 3372-3385

Transactions of Nonferrous Metals Society of China

www.tnmsc.cn



Adsorption behaviors and mechanisms of gold recovery from thiosulfate solution by ion exchange resin

Zhong-lin DONG, Tao JIANG, Bin XU, Qian LI, Yong-bin YANG

School of Minerals Processing and Bioengineering, Central South University, Changsha 410083, China

Received 25 March 2023; accepted 15 August 2023

Abstract: The adsorption behaviors and mechanisms of gold from thiosulfate solution on strong-base anion exchange resin were systematically investigated. The comparison experiment of adsorption ability and selectivity for gold showed that gel Amberlite IRA-400 resin with Type I quaternary ammonium functional group had better adsorption performance. The increases of resin dosage, ammonia concentration and solution pH were favorable to gold adsorption, whereas the rises of cupric and thiosulfate concentrations were disadvantageous to gold loading. Microscopic characterization results indicated that gold was adsorbed in the form of $[Au(S_2O_3)_2]^{3-}$ complex anion by exchanging with the counter ion Cl^- in the functional group of the resin. Density functional theory calculation result manifested that gold adsorption was mainly depended on the hydrogen bond and van der Waals force generated between O atom in $[Au(S_2O_3)_2]^{3-}$ and H atom in the quaternary ammonium functional group of the resin.

Key words: gold; thiosulfate solution; resin adsorption; behaviors and mechanisms; density functional theory calculation

1 Introduction

Gold is widely used in electronics, chemical, aerospace, medical, national defense and other fields [1–3]. Cyanidation has long been dominant in gold extraction due to its advantages of mature process and low cost [4,5]. However, cyanide is highly toxic, and the treatment of cyanide-containing waste water and waste residue puts great environmental pressure on gold enterprise [6–9]. In addition, the method is generally ineffective for gold extraction from refractory gold ore containing carbon and copper [10,11]. Therefore, the development of non-cyanide gold extraction method is a general trend.

At present, the main non-cyanide gold extraction methods include thiourea [12,13], chloride [14,15], thiocyanate [16,17], glycine

[18,19] and thiosulfate [20,21]. Among them, thiosulfate is widely considered the most promising because of its advantages of non-toxic reagent, quick leaching rate, weak corrosivity to equipment and being insensitive to impurities such as carbon and copper [22]. Nevertheless, numerous studies have shown that it is difficult to recover gold from thiosulfate solution due to the simultaneous existence of many kinds of metal ions (Au and Cu) and ligands ($S_2O_3^{2-}$, NH₃ and OH⁻) [23,24].

Precipitation [25], electrodeposition [26], solvent extraction [27], photocatalytic reduction [28], activated carbon adsorption [29], mesoporous silicon adsorption [30] and resin adsorption [31] are the primary methods of gold recovery from thiosulfate solution. Nevertheless, precipitation has the disadvantages of high metal powder consumption, low gold product purity and difficult barren solution recycling [32]. Electrodeposition

suffers from low current efficiency, high energy consumption and low product purity [33]. Solvent extraction is generally suitable for treating clarified solutions with high gold concentration, and the selective extraction of gold is also difficult [34]. The particle size of the used molybdenite material in photocatalytic reduction is nanoscale, leading to the difficulty of subsequent solid-liquid separation [35]. Activated carbon has extremely low affinity for $[Au(S_2O_3)_2]^{3-}$ and thus it is unsuitable for recovering gold from thiosulfate solution. The gold-loading capacity of modified activated carbon is evidently improved, but toxic modification reagents are used [36]. Mesoporous silicon has high gold-loading capacity, but its particle size is also small and thus the solid-liquid separation is difficult. In addition, Na+ exhibits serious negative effect on gold adsorption, which means that only the much more expensive (NH₄)₂S₂O₃ rather than cheap Na₂S₂O₃ can be used in gold leaching, therefore greatly increasing the gold extraction cost [37].

Compared with the above methods, resin adsorption is a better choice owing to its fast adsorption speed, high loading capacity, low requirements on the solution clarity and easy solid-liquid separation [1]. However, previous studies were mainly focused on the difference of gold-loading capacity among different types of resins [20], and there has been less systematic study on the key factors affecting gold adsorption such as cupric, ammonia, thiosulfate and solution pH. Furthermore, little research has been performed on the mechanism of gold adsorption on the resin such as the gold adsorption form, adsorption force and action atom. The above problems hinder the application of resin adsorption method for gold recovery from thiosulfate solution.

In this study, the adsorption behaviors and mechanisms of gold from thiosulfate solution on strong-base anion exchange resin were deeply and systematically researched. First, a suitable resin was selected from several typical gold adsorption resins based on their differences of adsorption ability and selectivity for gold. Then, the effects of resin dosage, solution pH and concentrations of cupric, ammonia and thiosulfate on gold adsorption were systematically studied. Finally, microscopic characterization and density functional theory (DFT) calculation were adopted to deeply explore

the mechanism of gold adsorption on the resin. Especially, the prevailing DFT method was adopted to reveal the gold adsorption mechanism at the atomic level. The research result will effectively promote the industrial application of thiosulfate process for gold extraction.

2 Experimental

2.1 Material and reagents

Weak-base resins have low gold-loading capacities when they are used for recovering gold from thiosulfate solution [21]. Thus, four typical strong-base resins were selected in this study and their appearances are shown in Figs. S1 in Supporting Information (SI), and their main physicochemical properties are displayed Table 1. Amberlite IRA-400 and Amberlite IRA-410 were gel resins that were yellow and milky white transparent spherical particles, whereas Amberlite IRA-900 and Amberlite IRA-910 resins were macroporous resins which were light yellow and milky white opaque spherical particles. In addition, the two gel/macroporous resins had the same loading capacity but different types of quaternary ammonium functional groups, as presented in Figs. S2 in SI.

Table 1 Main physicochemical properties of four strong-base anion exchange resins

Resin	Туре	Functional group	Loading capacity/ (meq·mL ⁻¹)
Amberlite IRA-400	Gel	Type I quaternary ammonium	1.4
Amberlite IRA-410	Gel	Type II quaternary ammonium	1.4
Amberlite IRA-900	Macroporous	Type I quaternary ammonium	1.0
Amberlite IRA-910	Macroporous	Type II quaternary ammonium	1.0

2.2 Experimental methods

Unless otherwise noted, for each adsorption experiment, 200 mL simulated thiosulfate solution was prepared and its initial compositions are as follows: [Au] 20 mg/L, [Cu²⁺] 0.02 mol/L, [NH₃] 1 mol/L and $[S_2O_3^2]$ 0.2 mol/L. First, 2 mL HAuCl₄

solution ([Au] 2 g/L) was transferred into a 300 mL beaker and the pH was regulated to be 6-7 with 0.5 mol/L NaOH solution. Then, 9.928 g Na₂S₂O₃· 5H₂O was added to react with [AuCl₄] to form [Au(S₂O₃)₂]³⁻complex. Meanwhile, 1 g CuSO₄·5H₂O and 15 mL NH₃·H₂O were successively added into another beaker to generate [Cu(NH₃)₄]²⁺ complex. Finally, $[Au(S_2O_3)_2]^{3-}$ and $[Cu(NH_3)_4]^{2+}$ solutions were mixed to prepare synthetic thiosulfate solution whose pH was adjusted to be 11.0 with 1 mol/L H₂SO₄ solution. At the beginning of the adsorption test, 0.5 g resin was added into the solution which was then agitated at 300 r/min with magnetic stirrer at 25 °C. 0.5 mL solution was regularly taken out during the adsorption to detect the gold and copper concentrations for drawing adsorption curves.

2.3 Analytical methods

The gold and copper concentrations in solutions were detected by an inductively coupled plasma optical emission spectrometer (ICP-OES, Optima 5300DV, PerkinElmer, USA). The surface composition and morphology of the resins were characterized with an scanning electron microscope (SEM, MIRA3 LMS, TESCAN Brno,s,r.o., Czech Republic) equipped with an energy dispersive spectroscope (EDS, Xplore30, Oxford Instruments). The Fourier transform infrared spectroscopy (FTIR, Nicolet iS50, Thermo Fisher Scientific, USA) was utilized to characterize the resins. The spectra were recorded in the 4000-400 cm⁻¹ region on samples dispersed in KBr. The chemical composition and accompanying changes of valence state on surface of the resins were identified through an X-ray photoelectron spectrometer (XPS, ESCALAB 250Xi, Thermo Fisher Scientific, USA). DFT calculation was carried out using Gaussian 16 program at B3LYP/6-311+G(d)level DFT-D3 corrections, and wave function analysis was performed with Multiwfn 3.6 program [38].

3 Results and discussion

3.1 Resin selection

3.1.1 Adsorption ability for gold

To obtain the suitable resin for gold adsorption, the adsorption abilities of four resins for gold in the thiosulfate solution were compared. The compositions of the used simulated solution were: [Au] 20 mg/L, [Cu²⁺] 0.02 mol/L, [NH₃] 1 mol/L,

 $[S_2O_3^{2-}]$ 0.2 mol/L and pH 11.0. The resin dosage was 2.5 g/L, and the results are shown in Fig. 1. As displayed in Fig. 1(a), the gold concentrations in residual gold-containing solutions first decreased with the increase of adsorption time and the decline extent of gold concentration was the largest for Amberlite IRA-400 resin, indicating its fastest adsorption rate. However, when the adsorption time was beyond 60 min, the gold concentrations basically stopped falling, because the limited active

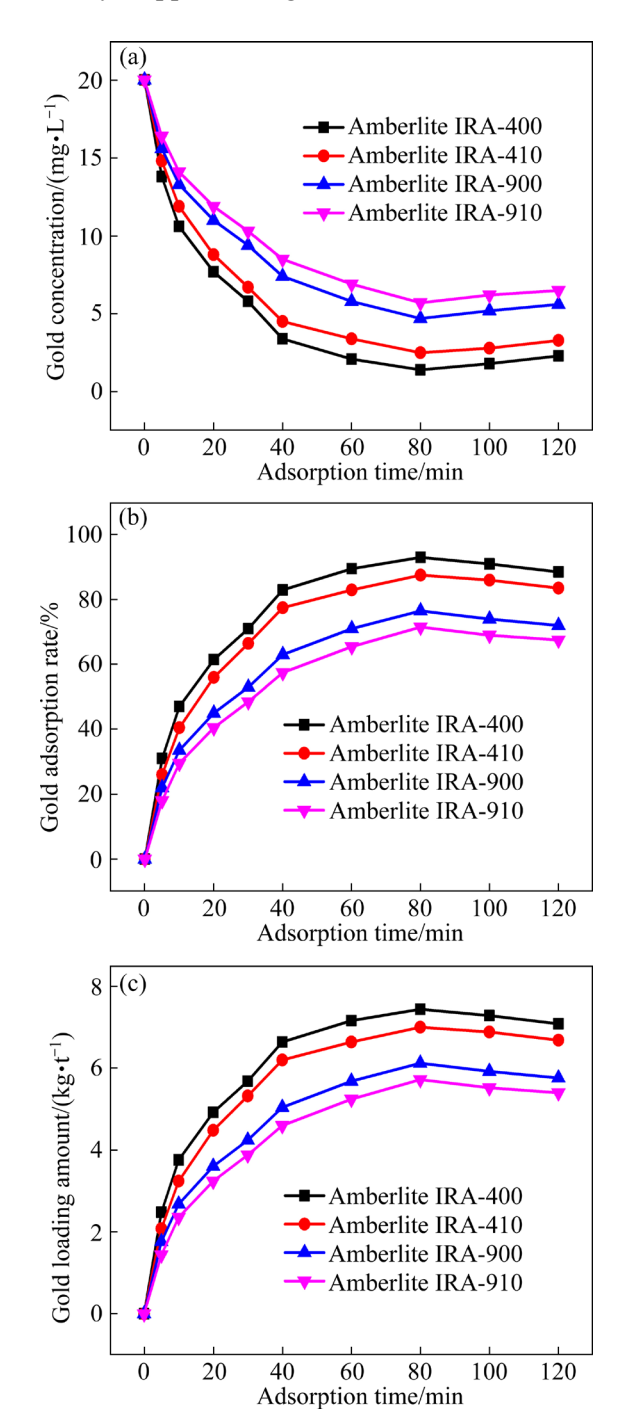


Fig. 1 Variations of gold concentration (a), adsorption rate (b) and loading amount (c) with adsorption time for four resins

site of the resin was completely occupied by the anions in the solution.

There were slight increases in the gold concentrations after 80 min, meaning that some of the gold on the resins was returned to the solution. This may be because that this part of adsorbed gold was displaced by high concentration of polythionates (mainly $S_3O_6^{2-}$ and $S_4O_6^{2-}$) originated from the gradual oxidation of $S_2O_3^{2-}$ by $[Cu(NH_3)_4]^{2+}$ with the augmented adsorption time [21]. Correspondingly, the gold adsorption rate and loading amounts of four resins rose with time and achieved the highest points at 80 min, after which they descended slightly, as presented in Figs. 1(b, c). Based on the above results, Amberlite IRA-400 resin possessed the strongest adsorption ability for gold.

3.1.2 Adsorption selectivity for gold

For thiosulfate leaching of gold, cupric ion is generally added to promote gold dissolution. Also, copper-containing associated minerals can be inevitably dissolved during leaching. Thus, copper ion concentration is usually high for the actual thiosulfate solution, and part of the them exists as $[Cu(S_2O_3)_3]^{5-}$. It is well-known that both copper and gold are Group IB elements which have the same numbers of outermost electron and are chemically similar. As the center atom for forming $[Cu(S_2O_3)_3]^{5-}$ and $[Au(S_2O_3)_2]^{3-}$ complexes, copper and gold have the same charge of plus one and electron configuration. Also, they have the same $S_2O_3^{2-}$ ligand and S coordinating atom. Thus, the two complexes have similar geometry configuration. Moreover, the adsorption reaction of $[Cu(S_2O_3)_3]^{5-}$ and $[Au(S_2O_3)_2]^{3-}$ on the resin occurs between O atom in $S_2O_3^{2-}$ of the two complexes and H atom in the quaternary ammonium functional groups of the resin. Therefore, $[Cu(S_2O_3)_3]^{5-}$ and $[Au(S_2O_3)_2]^{3-}$ have similar adsorption property. Based on the above analysis, [Cu(S₂O₃)₃]⁵⁻ has similar physicochemical properties with [Au(S₂O₃)₂]³⁻, and thus it can compete with gold for active sites of the resin. Therefore, the adsorption of four resins for copper was also considered.

As exhibited in Figs. 2(a-c), the adsorption rules of copper were similar to those of gold for four resins, i.e., as the adsorption proceeded, the copper concentrations in residual gold-containing solutions first decreased to the lowest values and then increased gradually, and the adsorption rates

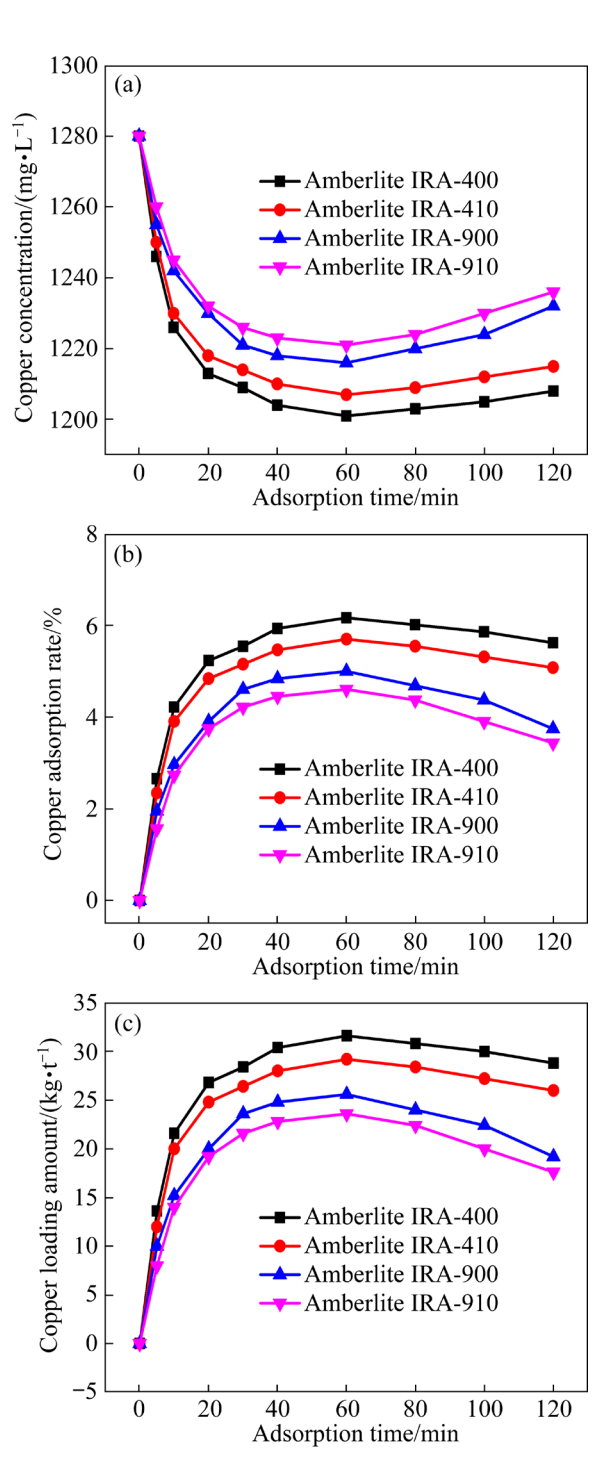


Fig. 2 Variations of copper concentration (a), adsorption rate (b) and loading amount (c) with adsorption time for four resins

and loading amounts showed the adverse trend. Among the four resins, Amberlite IRA-400 resin had the strongest adsorption ability for copper. Compared with Fig. 1, the copper adsorption rate was much lower than that of gold, because only a small part of copper in the solution occurred as $[Cu(S_2O_3)_3]^{5-}$ anion, and most of the copper existed

as $[Cu(NH_3)_4]^{2+}$ cation that could not be adsorbed. However, the copper loading amount was larger than that of gold since compared with $[Au(S_2O_3)_2]^{3-}$, $[Cu(S_2O_3)_3]^{5-}$ concentration was higher due to its evidently higher initial concentration. Furthermore, the decreases of adsorption rates and loading amount of copper were more pronounced, because the affinity of the resin for $[Cu(S_2O_3)_3]^{5-}$ was weaker than that for $[Au(S_2O_3)_2]^{3-}$, and thus it is easier for the adsorbed copper to be replaced.

Selectivity coefficient [39], the ratio of distribution coefficient, K_d (Eq. (1)), was used to quantify the selectivity of four resins for gold adsorption:

$$K_{\rm d} = \left(\frac{C_0}{C_{\rm e}} - 1\right) \cdot \frac{V}{M} \tag{1}$$

where C_0 is the initial gold/copper concentration, mg/L; Ce is the gold/copper concentration after adsorption equilibrium, mg/L; V is the solution volume, mL; M is the mass of the resin, g. As indicated in Table 2, the selectivity coefficients of four resins were all greater than 1, so they were all selective for gold adsorption. Nevertheless, the selectivity coefficient of Amberlite IRA-400 resin achieved 203.8, which was much higher than that of the remaining three resins. Therefore, Amberlite IRA-400 resin had the best selectivity for gold adsorption. Based on the above results of adsorption ability and selectivity of four strongbase resins, Amberlite IRA-400 resin possessed the optimal adsorption ability and selectivity for gold, and thus it was used to study the behaviors and mechanisms of gold adsorption.

The reason that Amberlite IRA 400 resin exhibited the optimal adsorption performance for gold in thiosulfate solution can be explained as follows. First, the loading capacity of Amberlite IRA 400 and Amberlite IRA 410 resins was 1.4 meg/mL that was higher than that (1.0 meg/mL) of Amberlite IRA 900 and Amberlite IRA 910 resins. This indicated that Amberlite IRA 400 and Amberlite IRA 410 resins had more active sites for gold adsorption, i.e., their theoretical gold loading amounts were higher, which was supported by the experimental result in Table 2. Furthermore, compared with Amberlite IRA 410 resin, Amberlite IRA 400 resin had better selectivity for gold, which might be because its pore radius was closer to the size of $[Au(S_2O_3)_2]^{3-}$, making it easier for

 $[Au(S_2O_3)_2]^{3-}$ to diffuse from the pore in the resin surface into its interior.

Table 2 Experimental results of gold adsorption by four resins

Resin	Equilibrium concentration/ (mg·L ⁻¹)		Distribution coefficient		Selectivity coefficient
	Gold	Copper	Gold	Copper	
Amberlite IRA-400	1.4	1201	5.3	0.026	203.8
Amberlite IRA-410	2.5	1207	2.8	0.024	116.7
Amberlite IRA-900	4.7	1216	1.3	0.021	61.9
Amberlite IRA-910	5.7	1221	1.0	0.019	52.6

For the resin loaded with copper and gold, the selective pre-desorption of copper could be realized using NH₃·H₂O+(NH₄)₂SO₄ or (NH₄)₂S₂O₃ solution, during which gold was not desorbed. After that, the gold on the resin could be efficiently desorbed with the mixed solution of Na₂SO₃ and NaCl.

3.2 Behaviors of gold adsorption on resin

3.2.1 Effect of resin dosage

The effect of resin dosage on gold adsorption is presented in Fig. 3. When the resin dosage was 1 g/L, the gold concentration initially decreased rapidly. However, when the adsorption time was beyond 30 min, the adsorption curve basically remained steady, indicating that the resin no longer absorbed gold. With small dosage, the active sites

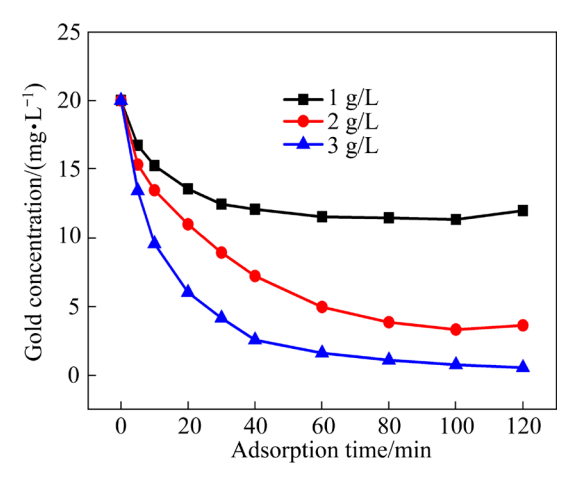


Fig. 3 Effect of resin dosage on gold adsorption (Solution compositions: [Au] 20 mg/L, [Cu²⁺] 0.02 mol/L, [NH₃] 1 mol/L, $[S_2O_3^{2-}]$ 0.2 mol/L and pH 11.0)

of the resin were quickly occupied by the anions such as $[Au(S_2O_3)_2]^{3-}$, $[Cu(S_2O_3)_3]^{5-}$ and $S_2O_3^{2-}$ in the solution, and the adsorption quickly reached the saturation. With the increase of resin dosage, the decrease rate of gold concentration accelerated. This indicated that the gold adsorption performance was improved, which was attributed to the increase of active sites for gold loading. After adsorption for 120 min at the resin dosage of 3 g/L, the gold concentration dropped from initial 20 to 0.56 mg/L. The above results showed that the increase of resin dosage was beneficial to gold adsorption.

3.2.2 Effect of cupric concentration

The effect of Cu²⁺ concentration on gold adsorption is shown in Fig. 4. When the Cu²⁺ concentration was 0.01 mol/L, gold concentration declined rapidly, i.e., the adsorption rate was quick. After 60 min, the gold concentration decreased to 9.59 mg/L. With the prolongation of adsorption time, the gold adsorption was not effectively improved, and absorption equilibrium achieved basically. As Cu²⁺ concentration augmented, the decrease rate of gold concentration became slower, which was ascribed to the increase of the concentration of [Cu(S₂O₃)₃]⁵⁻ impurity anion that can compete with $[Au(S_2O_3)_3]^{3-}$. After adsorption for 120 min at 0.03 mol/L Cu²⁺, the gold concentration only descended to 14.68 mg/L. The above results showed that the increase of Cu²⁺ concentration was unbeneficial to gold adsorption.

3.2.3 Effect of ammonia concentration

The effect of NH₃ concentration on gold adsorption is shown in Fig. 5. As NH₃ concentration increased from 0.5 to 2 mol/L, the decrease rate of

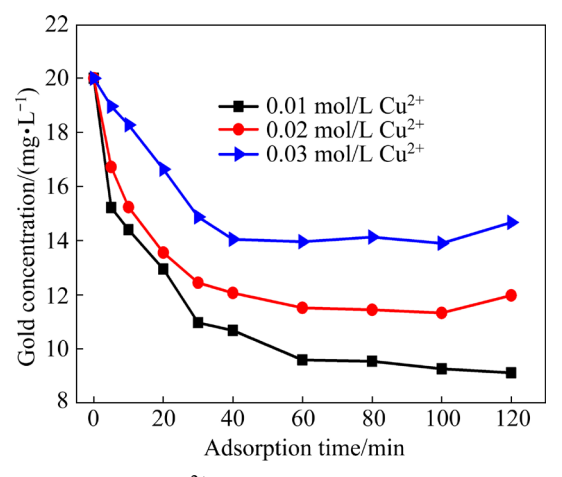


Fig. 4 Effect of Cu^{2+} concentration on gold adsorption (Solution compositions: [Au] 20 mg/L, [NH₃] 1 mol/L, [S₂O₃²⁻] 0.2 mol/L and pH 11.0)

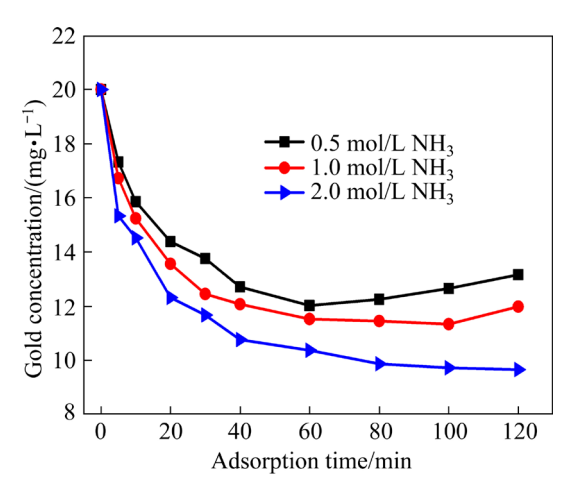


Fig. 5 Effect of NH₃ concentration on gold adsorption (Solution compositions: [Au] 20 mg/L, [Cu²⁺] 0.02 mol/L, [S₂O₃²⁻] 0.2 mol/L and pH 11.0)

gold concentration became quicker, meaning that the gold adsorption was easier. In fact, S₂O₃²⁻ and NH₃ can separately complex with Cu(I) and Cu(II) to form [Cu(S₂O₃)₃]⁵⁻ and [Cu(NH₃)₄]²⁺, the two main forms of copper ions in the solution. At higher NH₃ concentration, more copper exists as [Cu(NH₃)₄]²⁺ cation that cannot be adsorbed by the resin, therefore improving gold adsorption. The above results manifested that the increase of NH₃ concentration was advantageous to gold adsorption. 3.2.4 Effect of thiosulfate concentration

The effect of $S_2O_3^{2-}$ concentration on gold adsorption is exhibited in Fig. 6. As $S_2O_3^{2-}$ concentration rose from 0.1 to 0.3 mol/L, the decrease rate of gold concentration became slower, indicating that gold adsorption was hindered. Two reasons can be accounted for the result. First, at

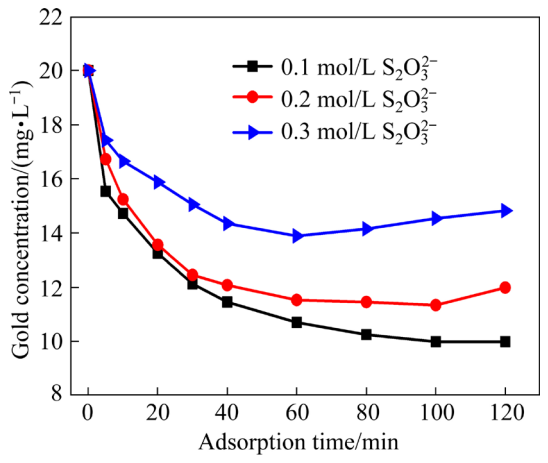


Fig. 6 Effect of $S_2O_3^{2-}$ concentration on gold adsorption (Solution compositions: [Au] 20 mg/L, [Cu²⁺] 0.02 mol/L, [NH₃] 1 mol/L and pH 11.0)

higher $S_2O_3^{2-}$ concentration, more copper exists as $[Cu(S_2O_3)_3]^{5-}$ anion that can easily occupy the finite active sites of the resin. Second, $S_2O_3^{2-}$ itself is an anion which can also compete for gold adsorption on the resin. The above results showed that the increase of $S_2O_3^{2-}$ concentration was disadvantageous to gold adsorption.

3.2.5 Effect of solution pH

The effect of solution pH on gold adsorption is displayed in Fig. 7. When solution pH augmented from 9.0 to 11.0, the decrease rate of gold concentration was quicker. This is because the increase of solution pH shifts the ionization equilibrium of ammonia to the left (Eq. (2)), which benefits the stability of NH₃. As a result, the concentration of [Cu(S₂O₃)₃]⁵⁻ anion decreased, thus promoting gold adsorption. In addition, with the increase of adsorption time, S₂O₃²⁻ can be oxidized by [Cu(NH₃)₄]²⁺ into polythionates that can exert strong competitive adsorption with $[Au(S_2O_3)_2]^{3-}$ on the resin. At higher solution pH, the stability of $S_4O_6^{2-}$ declined and was decomposed into $S_2O_3^{2-}$ and SO_3^{2-} that had evidently weaker competitive adsorption with $[Au(S_2O_3)_2]^{3-}$ compared with $S_4O_6^{2-}$, which also improved gold adsorption. The above results demonstrated that the increase of solution pH was conducive to gold adsorption.

$$NH_3 \cdot H_2O \Longrightarrow NH_4^+ + OH^-$$
 (2)

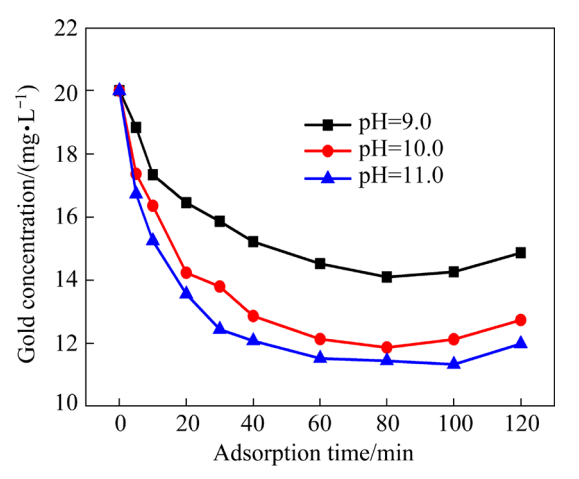


Fig. 7 Effect of solution pH on gold adsorption (Solution compositions: [Au] 20 mg/L, [Cu²⁺] 0.02 mol/L, [NH₃] 1 mol/L and [S₂O₃²⁻] 0.2 mol/L)

3.3 Mechanisms of gold adsorption on resin

3.3.1 Microscopic characterization

3.3.1.1 SEM-EDS analysis

To investigate the adsorption mechanism of

gold on the strong-base resin, SEM-EDS analyses on the origin resin and gold-loaded resin were first performed, and the results are shown in Fig. 8. The original resin was yellow (Fig. 8(a)), its surface was relatively flat and only some small holes were observed (Fig. 8(c)), because it is a gel type resin which will swell enough to open up the holes in its surface when it is placed in aqueous solution. C, N, O and Cl elements were detected in the EDS spectrum (Fig. 8(e)).

After the resin was loaded with gold, its color became dark yellow (Fig. 8(b)), and there was a dense uneven covering layer on the surface where no holes were found (Fig. 8(d)) since they were occupied by the anions in the solution. The peaks of Au and S elements appeared while those of Cl element disappeared in the EDS spectrum (Fig. 8(f)), indicating that gold was adsorbed through the exchange reaction between $[Au(S_2O_3)_2]^{3-}$ in the solution and Cl^- on the functional group of the resin.

3.3.1.2 FTIR analysis

The infrared spectra of the original resin and gold-loaded resin are exhibited in Fig. 9. The resin had abundant groups [40]. The peak at 3381 cm⁻¹ corresponded to O-H stretching vibration of hygroscopic water. The peak at 3020 cm⁻¹ was assigned to C-H stretching vibrations of benzene rings. The peak at 2922 cm⁻¹ was attributed to asymmetric C-H stretching vibrations of CH₂ and CH_3 in CH_3 —N. The peak at $1615\,cm^{-1}$ corresponded to C=C stretching vibrations of benzene rings and deformation vibrations of — $CH_2 - N^+(CH_3)_3Cl^-$. The peaks at 1484.36, 1220.01 and 1125.67 cm⁻¹ were assigned to C-N stretching vibrations of -CH₂-N⁺(CH₃)₃Cl⁻. The peaks at 976.15, 924.97 and 707.87 cm⁻¹ were attributed to C — H out-of-plane deformation vibrations of benzene rings.

When gold was adsorbed on the resin, new peaks appeared at 528.74, 652.95 and 629.71 cm⁻¹. The first two peaks were assigned to the characteristic vibrations of S—S and S—O bonds in S₂O₃², and the third one was Au—S bond in [Au(S₂O₃)₂]³-, indicating that gold was adsorbed in the form of [Au(S₂O₃)₂]³-. Moreover, the peak of quaternary ammonium functional group at 1125.67 moved to 1107.48 cm⁻¹, which showed that the functional group involved the gold adsorption.

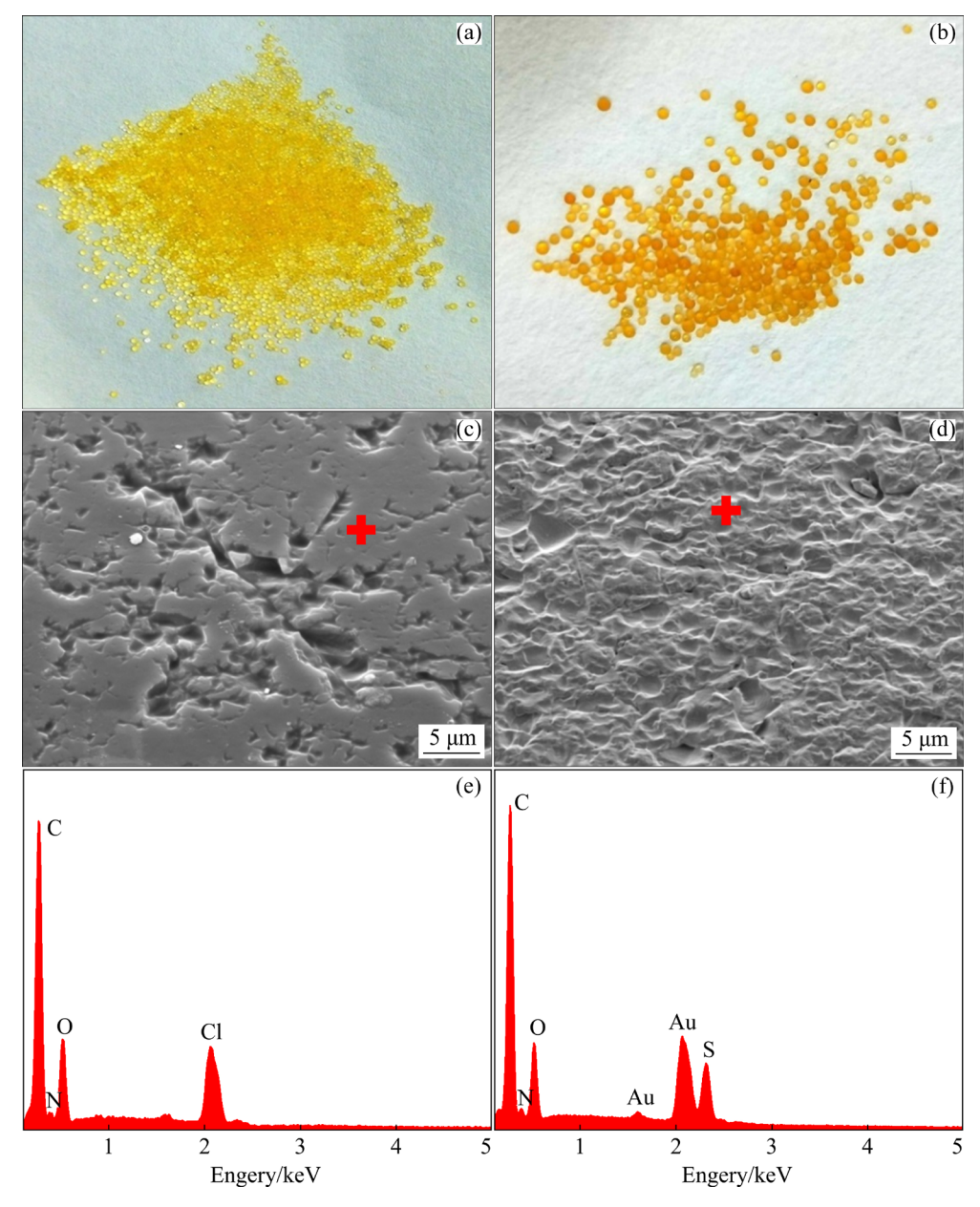


Fig. 8 Appearances (a, b), SEM images (c, d) and EDS spectra (e, f) of original (a, c, e) and gold-loaded (b, d, f) resins

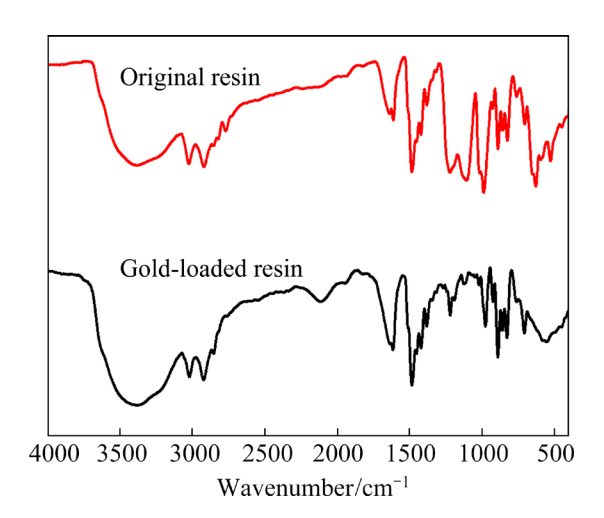
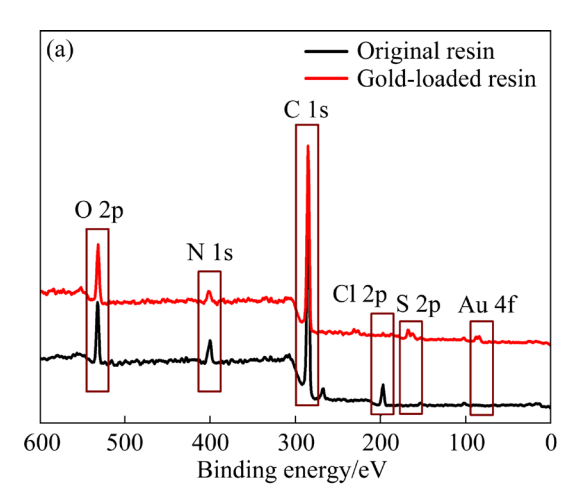
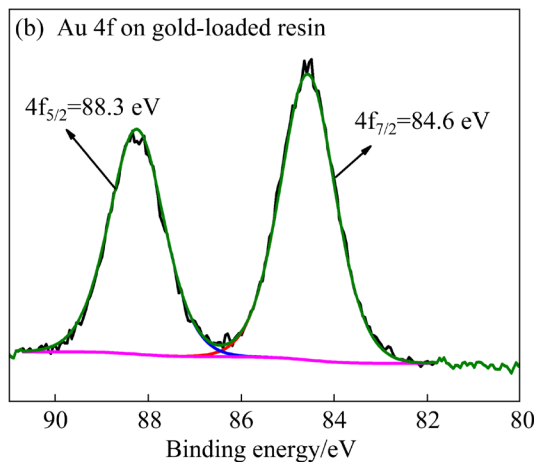


Fig. 9 Infrared spectra of original and gold-loaded resins

3.3.1.3 XPS analysis

The XPS analysis results of the origin resin and gold-loaded resin are displayed in Fig. 10. As shown in Fig. 10(a), for the original resin, the peaks at the binding energies of 531.8, 399.8, 284.8 and 197.1 eV were separately attributed to O 1s, N 1s, C 1s and Cl 2p. As for the gold-loaded resin, the new peaks of Au 4f and S 2p appeared at the binding energies of 84.8 and 167.8 eV, respectively, whereas the peak of Cl 2p disappeared. The above results proved that gold was successfully adsorbed on the resin through the exchange reaction between [Au(S₂O₃)₂]³⁻ in the solution and Cl⁻ on the functional groups of the resin, which was in





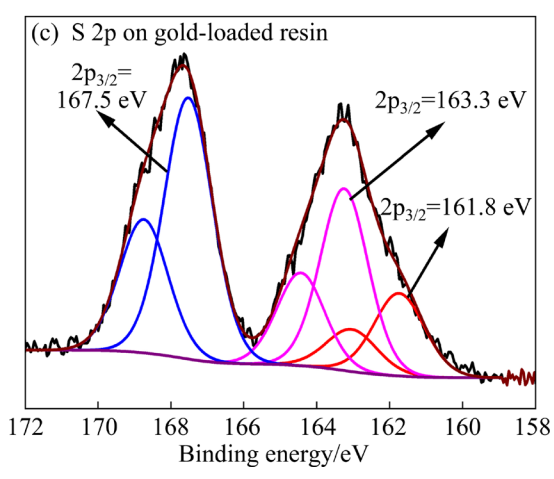


Fig. 10 Full XPS spectra of original resin and gold-loaded resin (a) and Au 4f (b) and S 2p (c) XPS spectra of gold-loaded resin

agreement with the EDS analysis results.

The peak-differentiation-imitating results of Au 4f and S 2p XPS spectra of the gold-loaded resin are exhibited in Figs. 10(b, c). The peaks at the binding energies of 88.3 and 84.6 eV were assigned to Au $4f_{5/2}$ and Au $4f_{7/2}$, respectively, which was typically Au(I) [29]. This indicated that gold

adsorbed on the resin was still Au(I) without any state change in $[Au(S_2O_3)_2]^{3-}$. Three binding energy peaks of S $2p_{3/2}$ appeared at 161.8, 163.3 and 167.5 eV. The peaks at 161.8 and 167.5 eV were attributed to S²⁻ and S⁶⁺ in S₂O₃²⁻, and the peak at 163.3 eV was assigned to S⁰ in elemental sulfur that was derived from S₂O₃²⁻ decomposition.

3.3.2 DFT calculation

3.3.2.1 Binding energy calculation

DFT calculation was performed to study the adsorption mechanism of gold on the strong-base resin at the atomic level. The optimized configurations of Cl⁻ and $[Au(S_2O_3)_2]^{3-}$ adsorption on Amberlite IRA-400 resin are shown in Fig. S3 in SI. The binding energies ($E_{Binding}$) of the configurations can be calculated using Eq. (3):

$$E_{\text{Binding}} = E_{\text{A}+\text{B}} - E_{\text{A}} - E_{\text{B}} \tag{3}$$

where E_{A+B} is the single point energy of adsorption configuration, and E_A and E_B are the single point energies of $Cl^-/[Au(S_2O_3)_2]^{3-}$ and Amberlite IRA-400 resin, respectively [41-43]. If the binding energy is negative, the adsorption reaction can occur spontaneously. The greater the absolute value of the negative value is, the easier the adsorption reaction is to happen. The calculation results of binding energy are displayed in Tables 3 and 4.

The binding energies of Amberlite IRA-400 resin for Cl⁻ and $[Au(S_2O_3)_2]^{3-}$ are -137.85 and -157.53 kJ/mol, respectively, and thus the resin can adsorb the two anions. Moreover, the binding energy of the resin for $[Au(S_2O_3)_2]^{3-}$ is more negative, and thus this adsorption reaction is more likely to occur, which is in accordance with the result that the counter ion Cl⁻ on the functional group of the resin could be replaced by $[Au(S_2O_3)_2]^{3-}$ in the thiosulfate solution.

Table 3 Calculation result of binding energy of Cl⁻adsorption on Amberlite IRA-400 resin

Configuration	Single point energy (kJ·mol ⁻¹)	Binding energy for one Cl ^{-/} (kJ·mol ⁻¹)	Binding energy for three Cl ^{-/} (kJ·mol ⁻¹)
Cl ⁻	-1208768.59		
Amberlite IRA-400 resin	-7132491.85	-45.95	-137.85
Adsorption configuration	-8341216.39		

Table 4 Calculation result of binding energy of $[Au(S_2O_3)_2]^{3-}$ adsorption on Amberlite IRA-400 resin

Configuration	Single point energy (kJ·mol ⁻¹)	Binding energy/ (kJ·mol ⁻¹)
$[Au(S_2O_3)_2]^{3-}$	-5724391.57	
Amberlite IRA-400 resin	-7132491.85	-157.53
Adsorption configuration	-12857040.94	

3.3.2.2 Atom charge analysis

Mulliken distributions The charge $[Au(S_2O_3)_2]^{3-}$, resin and adsorption configuration are shown in Tables S1-S3 in SI, and the corresponding atomic numbers are displayed in Figs. S4–S6 in SI. For $[Au(S_2O_3)_2]^{3-}$, the O atoms in $S_2O_3^{2-}$ (O3, O4, O6, O7, O10 and O11) have high negative charges. As for the resin, the H atoms in -CH₃ of quaternary ammonium functional group and adjacent -CH₂- (H98, H99, H100, H101, H127, H128, H129, ..., H166) possess high positive charges. Thus, these O and H atoms are more likely to attract each other. Furthermore, the net charges of $[Au(S_2O_3)_2]^{3-}$ and resin are -3 and +4 before adsorption, while those become -2.93 and +3.93 after adsorption. Therefore, the electron transfer occurs during the adsorption, indicating that the mutual interaction exists between $[Au(S_2O_3)_2]^{3-}$ and the resin.

3.3.2.3 Electron density difference analysis

The mutual interaction between $[Au(S_2O_3)_2]^{3-}$ and resin can cause the electron redistribution, and thus the electron density difference map of $[Au(S_2O_3)_2]^{3-}$ adsorption on Amberlite IRA-400 resin was plotted, as displayed in Fig. 11. The blue and purple isosurfaces represent the regions where electron density is increased and decreased after the interaction between $[Au(S_2O_3)_2]^{3-}$ and resin, respectively.

Purple isosurfaces appear around the two O atoms (O172 and O173) of S₂O₃² near the quaternary ammonium functional group of resin. This indicates that the electron densities of the regions drop, i.e., the electrons transfer outward. Meanwhile, directly opposite the two O atoms, purple isosurfaces are observed round the two H atoms ((H100 and H164)) on the —CH₃ of the functional group and the adjacent — CH₂ —, showing that the electron densities of the regions are also decreased. Theoretically, the electron

densities between the two O atoms and opposite two H atoms are very small when only [Au(S₂O₃)₂]³⁻ or Amberlite IRA-400 resin is present. However, in adsorption configuration, blue isosurfaces occur between the two O atoms and opposite two H atoms, indicating the increase of electron density in the regions. This is because the electrons transfer from O and H atoms to the regions. Moreover, of the two blue isosurfaces, the one between the O atom of S₂O₃²⁻ and opposite H atom on the -CH₃ of the functional group is evidently larger, that is, the electron density increases more, showing that they are the main interaction atoms. Based on the above result, during gold adsorption, the main interaction atoms are O atom in $[Au(S_2O_3)_2]^{3-}$ and H atom on the —CH₃ of the quaternary ammonium group in the resin.

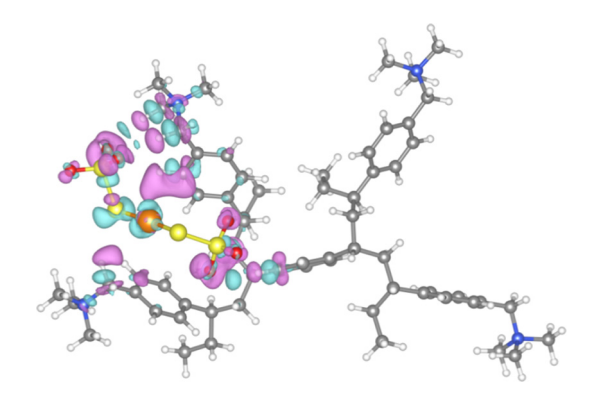


Fig. 11 Electron density difference map of $[Au(S_2O_3)_2]^{3-}$ adsorption on Amberlite IRA-400 resin

3.3.2.4 Electrostatic potential analysis

Electrostatic potential is a very important real space function for interpreting and predicting possible electrostatic interaction between a molecule and environmental molecules [44]. The potential map electrostatic can intuitively characterize the electrostatic potential distribution of molecule surface. The electrostatic potential maps of [Au(S₂O₃)₂]³⁻, resin and their adsorption configuration are shown in Fig. 12. The red and blue parts separately represent the regions in which the electrostatic potentials are negative and positive.

The surfaces of $[Au(S_2O_3)_2]^{3-}$ and resin are red and blue (Figs. 12(a, b)), which indicates that their electrostatic potentials are negative and positive. Moreover, the colors are darker at the positions of $S_2O_3^{2-}$ and quaternary ammonium functional group, which means that the electrostatic potentials of these two parts are more negative and positive. As a

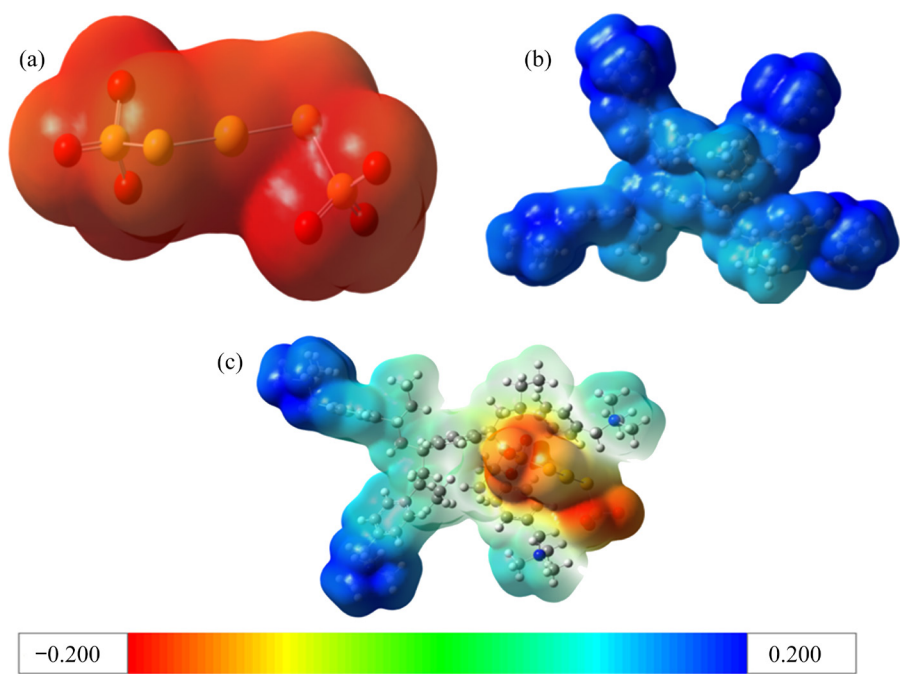


Fig. 12 Electrostatic potential maps of $[Au(S_2O_3)_2]^{3-}$ (a), Amberlite IRA-400 resin (b) and their adsorption configuration (c)

result, they are more likely to be the active sites where the adsorption reaction occurs, which makes the generated adsorption configuration more stable because of its lower energy. The electrostatic potential map in Fig. 12(c) further demonstrates this result. When the resin adsorbs $[Au(S_2O_3)_2]^{3-}$, the color of the interaction region is obviously lighter, i.e., the electrostatic potential here is significantly reduced. This is because the electrostatic potential is complementary as they approach each other. The surfaces of the two quaternary ammonium functional groups far away from the interaction region are still in dark blue since the mutual interaction between the functional group and $[Au(S_2O_3)_2]^{3-}$ is weak at a long distance, and the electrostatic potential change is small.

3.3.2.5 Independent gradient model analysis

Reduced density gradient (RDG) and independent gradient model (IGM) are the two most popular methods for analyzing the region and feature of weak interactions [45]. Compared with RDG, IGM is more convenient to analyze the interaction between molecules through user-defined fragments. Therefore, to identify and visualize the region and feature of weak interaction between [Au(S₂O₃)₂]³⁻ and resin, IGM analysis for their adsorption configuration was performed, and the result is shown in Fig. 13. The blue, green and red

isosurfaces represent hydrogen bond, van der Waals force and steric hindrance, respectively.

Two green isosurfaces appear between the two O atoms (O172 and O173) of [Au(S₂O₃)₂]³⁻ and two H atoms ((H100 and H164)) on the —CH₃ of functional group and the adjacent —CH₂—, which shows that there are obvious van der Waals forces between [Au(S₂O₃)₂]³⁻ and resin. Also, two small blue isosurfaces are observed on the green isosurfaces, so hydrogen bonds also exist. In fact, hydrogen bond occurs in molecules when a hydrogen atom bonded to a small electronegative atom attracts an electron pair on an electronegative atom on an adjacent molecule. Thus, hydrogen bonds (C68—H164···O173 and C30—H100···O172) can be formed.

Based on the above results, it can be concluded that $[Au(S_2O_3)_2]^{3-}$ adsorption on the resin is mainly realized through the interactions of van der Waals forces and hydrogen bonds generated between the O atoms in $[Au(S_2O_3)_2]^{3-}$ and H atoms on the —CH₃ of functional group and the adjacent —CH₂ in the resin. According to the above result of electron density difference analysis, the main interaction atom of the resin is the H atom on the —CH₃ of functional group. Therefore, gold adsorption on the resin primarily is depended on the hydrogen bond and van der Waals force formed

between the O atom in $[Au(S_2O_3)_2]^{3-}$ and H atom on the $-CH_3$ of quaternary ammonium functional group in the resin.

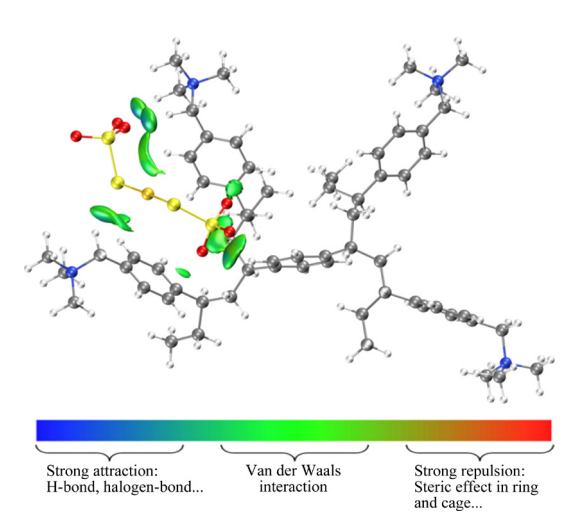


Fig. 13 Independent gradient model map of $[Au(S_2O_3)_2]^{3-}$ adsorption on Amberlite IRA-400 resin

4 Conclusions

- (1) The experimental results of adsorption ability and selectivity of four resins for gold indicated that among four strong-base resins, gel Amberlite IRA-400 resin with Type I quaternary ammonium functional group possessed the optimal loading ability and selectivity for gold in thiosulfate solution. The increase of resin dosage augmented the active site amount, and the rise of ammonia concentration and solution pH decreased the concentration of $[Cu(S_2O_3)_3]^{5-}$ that has strong competitive adsorption with $[Au(S_2O_3)_2]^{3-}$ on the resin, which thus were all favorable to gold adsorption. The increase of cupric and thiosulfate concentrations deteriorated gold adsorption due to the increase of $[Cu(S_2O_3)_3]^{5-}$ concentration.
- (2) The original resin contained C, N, O and Cl elements; Au and S elements occurred while Cl element disappeared in the EDS spectrum of gold-loaded resin. Meanwhile, Au—S, S—S and S—O bonds, and Au⁺, S²⁻ and S⁶⁺ were detected in the FTIR and XPS spectra of the gold-loaded resin. These results indicated that gold was adsorbed in the form of $[Au(S_2O_3)_2]^{3-}$ on the resin through exchanging with the counter ion Cl⁻ on the functional group of the resin.
- (3) The binding energy calculation result showed that the resin adsorbed $[Au(S_2O_3)_2]^{3-}$ more readily than Cl^- , and thus Cl^- on the functional

group of the resin could be substituted by $[Au(S_2O_3)_2]^{3-}$. Atom charge, electron density difference, electrostatic potential and independent gradient model analysis results indicated that the O atom in $[Au(S_2O_3)_2]^{3-}$ and H atom in the —CH₃ of quaternary ammonium group of the resin are the main interaction atoms where hydrogen bond and van der Waals force are formed for gold adsorption on the resin.

CRediT authorship contribution statement

Zhong-lin DONG: Conceptualization, Investigation, Writing – Original draft, Funding acquisition; Tao JIANG: Investigation, Formal analysis; Bin XU: Funding acquisition, Supervision, Resources, Validation; Qian LI: Supervision, Writing – Review & editing; Yong-bin YANG: Supervision, Writing – Review & editing

Declaration of competing interest

The authors declare that they have no known competing financial interests or personal relationships that could have appeared to influence the work reported in this paper.

Acknowledgments

The authors are thankful for the financial support from the Natural Science Foundation of Hunan Province, China (No. 2023JJ40723), China Postdoctoral Science Foundation (No. 2022M723549) and the National Natural Science Foundation of China (Nos. 52174271, 51504293).

Supporting Information

Supporting Information in this paper can be found at: http://tnmsc.csu.edu.cn/download/19-p3372-2023-0344-Supporting Information.pdf.

References

- [1] XIE Feng, CHEN Jun-nan, WANG Jian, WANG Wei. Review of gold leaching in thiosulfate-based solutions [J]. Transactions of Nonferrous Metals Society of China, 2021, 31(11): 3506–3529.
- [2] CAO Pan, ZHANG Shang-hua, ZHENG Ya-jie, HE Han-bing, LAI Shen-zhi, WANG Xing-jun, TAN Bing. Differences of cyanide leaching between calcine and dust from refractory gold concentrates [J]. Transactions of Nonferrous Metals Society of China, 2020, 30(7): 1964–1979.
- [3] YANG Yong-bin, ZHANG Xi, XU Bin, LI Qian, JIANG Tao, WANG Ya-xuan. Effect of arsenopyrite on thiosulfate leaching of gold [J]. Transactions of Nonferrous Metals Society of China, 2015, 25(10): 3454–3460.
- [4] HASHEMZADEHFINI M, FICERIOVÁ J, ABKHOSHK E,

- SHAHRAKI B K. Effect of mechanical activation on thiosulfate leaching of gold from complex sulfide concentrate [J]. Transactions of Nonferrous Metals Society of China, 2011, 21(12): 2744–2751.
- [5] LIU Wei-feng, YANG Tian-zu, XIA Xing. Behavior of silver and lead in selective chlorination leaching process of gold-antimony alloy [J]. Transactions of Nonferrous Metals Society of China, 2010, 20(2): 322–329.
- [6] HAN Wen-wen, YANG Hong-ying, TONG Lin-lin. Cyanide removal for ultrafine gold cyanide residues by chemical oxidation methods [J]. Transactions of Nonferrous Metals Society of China, 2022, 32(12): 4129–4138.
- [7] LI Qi, XIE Feng, CHANG Yong-feng, WANG Wei, ZHANG Li-bo. Behavior and mechanism of cyanide loss in ultrasound-assisted gold leaching process [J]. Transactions of Nonferrous Metals Society of China, 2023, 33(2): 609–618.
- [8] CHEN Xiang-yang, LAN Xin-zhe, ZHANG Qiu-li, ZHOU Jun, SONG Yong-hui. Behavior of S₂O₃²⁻ and SO₃²⁻ in sulfur-bearing aqueous solution system for gold leaching [J]. Transactions of Nonferrous Metals Society of China, 2010, 20(Suppl.): 46–49.
- [9] SITANDO O, SENANYAKE G, DAI X, NIKOLOSKI A N, BREUER P. A review of factors affecting gold leaching in non-ammoniacal thiosulfate solutions including degradation and in-situ generation of thiosulfate [J]. Hydrometallurgy, 2018, 178: 151–175.
- [10] FENG D, VAN DEVENTER J S J. Thiosulphate leaching of gold in the presence of ethylenediaminetetraacetic acid (EDTA) [J]. Minerals Engineering, 2010, 23: 143–150.
- [11] GROSSE A C, DICINOSKI G W, SHAW M J, HADDAD P R. Leaching and recovery of gold using ammoniacal thiosulfate leach liquors (A review) [J]. Hydrometallurgy, 2003, 69: 1–21.
- [12] LI J, MILLER J D. A review of gold leaching in acid thiourea solutions [J]. Mineral Processing and Extractive Metallurgy Review, 2006, 27: 177–214.
- [13] GUO Xue-yi, ZHANG Lei, TIAN Qing-hua, QING Hong. Stepwise extraction of gold and silver from refractory gold concentrate calcine by thiourea [J]. Hydrometallurgy, 2020, 194: 105330.
- [14] DONG Zhong-lin, JIANG Tao, XU Bin, YANG Jun-kui, CHEN Yan-zhu, YANG Yong-bin, LI Qian. Comprehensive recoveries of selenium, copper, gold, silver and lead from a copper anode slime with a clean and economical hydrometallurgical process [J]. Chemical Engineering Journal, 2020, 393: 124762.
- [15] XU Bin, CHEN Yan-zhu, DONG Zhong-lin, JIANG Tao, ZHANG Bang-sheng, LIU Gui-qing, YANG Jun-kui, LI Qian, YANG Yong-bin. Eco-friendly and efficient extraction of valuable elements from copper anode mud using an integrated pyro-hydrometallurgical process [J]. Resource Conservation & Recycling, 2021, 164: 105195.
- [16] WU Hao, FENG Yali, HUANG Wan-fu, LI Hao-ran, LIAO Sheng-de. The role of glycine in the ammonium thiocyanate leaching of gold [J]. Hydrometallurgy, 2019, 185: 111–116.
- [17] AZIZITORGHABEH A, WANG J X, RAMSAY J A, GHAHREMAN A. A review of thiocyanate gold leaching-Chemistry, thermodynamics, kinetics and processing [J]. Minerals Engineering, 2021, 160: 106689.

- [18] ORABY E A, EKSTEEN J J. The leaching of gold, silver and their alloys in alkaline glycine–peroxide solutions and their adsorption on carbon [J]. Hydrometallurgy, 2015, 152: 199–203.
- [19] ORABY E A, EKSTEEN J J, KARRECH A, ATTA M. Gold extraction from paleochannel ores using an aerated alkaline glycine lixiviant for consideration in heap and in-situ leaching applications [J]. Minerals Engineering, 2019, 138: 112–118.
- [20] ZHANG H G, DREISINGER D B. The adsorption of gold and copper onto ion-exchange resins from ammoniacal thiosulfate solutions [J]. Hydrometallurgy, 2002, 66: 67–76.
- [21] DONG Zhong-lin, JIANG Tao, XU Bin, YANG Yong-bin, LI Qian. An eco-friendly and efficient process of low potential thiosulfate leaching-resin adsorption recovery for extracting gold from a roasted gold concentrate [J]. Journal of Cleaner Production, 2019, 229: 387–398.
- [22] XU Bin, LI Ke, DONG Zhong-lin, YANG Yong-bin, LI Qian, LIU Xiao-liang, JIANG Tao. Eco-friendly and economical gold extraction by nickel catalyzed ammoniacal thiosulfate leaching-resin adsorption recovery [J]. Journal of Cleaner Production, 2019, 233: 1475–1485.
- [23] DONG Zhong-lin, JIANG Tao, XU Bin, ZHANG Bang-sheng, LIU Gui-qing, LI Qian, YANG Yong-bin. A systematic and comparative study of copper, nickel and cobalt-ammonia catalyzed thiosulfate processes for eco-friendly and efficient gold extraction from an oxide gold concentrate [J]. Separation and Purification Technology, 2021, 272: 118929.
- [24] XU Bin, LI Ke, LI Qian, YANG Yong-bin, LIU Xiao-liang, JIANG Tao. Kinetic studies of gold leaching from a gold concentrate calcine by thiosulfate with cobalt–ammonia catalysis and gold recovery by resin adsorption from its pregnant solution [J]. Separation and Purification Technology, 2019, 213: 368–377.
- [25] KARAVASTEVA M. Kinetics and deposit morphology of gold cemented on magnesium, aluminum, zinc, iron and copper from ammonium thiosulfate—ammonia solutions [J]. Hydrometallurgy, 2010, 104: 119–122.
- [26] KASPER A C, VEIT H M, GARCÍA-GABALDÓN M, HERRANZ V P. Electrochemical study of gold recovery from ammoniacal thiosulfate, simulating the PCBs leaching of mobile phones [J]. Electrochimica Acta, 2017, 259: 500-509.
- [27] ZHAO Jin, WU Zhi-chun, CHEN Jia-yong. Separation of gold from other metals in thiosulfate solutions by solvent extraction [J]. Separation and Purification Technology, 1999, 34: 2061–2068.
- [28] CHEN Peng, LIANG Yu-meng, YANG Bing-qiao, JIA Fei-fei, SONG Shao-xiao. In-situ reduction of Au(I) for efficient recovery of gold from thiosulfate solution by 3D MoS₂/Chitosan aerogel [J]. ACS Sustainable Chemistry & Engineering, 2020, 8: 3673–3680.
- [29] CHEN Yun-long, ZI Fu-ting, HU Xian-zhi, YANG Peng, MA Yong-ping, CHEN Hui-ling, WANG Qiang, QIN Xue-cong, LIU Yang, CHEN Shu-liang, WANG Chao-wu. The use of new modified activated carbon in thiosulfate solution: A green gold recovery technology [J]. Separation and Purification Technology, 2020, 230: 115834.

- [30] FOTOOHI B, MERCIER L. Some insights into the chemistry of gold adsorption by thiol and amine functionalized mesoporous silica in simulated thiosulfate system [J]. Hydrometallurgy, 2015, 156: 28–39.
- [31] ZHANG H G, DREISINGER D B. The recovery of gold from ammonical thiosulfate solutions containing copper using ion exchange resin columns [J]. Hydrometallurgy, 2004, 72: 225–234.
- [32] JEON S, TABELIN C B, PARK I, NAGATA Y, ITO M, HIROYOSHI N. Ammonium thiosulfate extraction of gold from printed circuit boards (PCBs) of end-of-life mobile phones and its recovery from pregnant leach solution by cementation [J]. Hydrometallurgy, 2019, 191: 105214.
- [33] CHOO W L, JEFFREY M I. An electrochemical study of copper cementation of gold(I) thiosulfate [J]. Hydrometallurgy, 2004, 71: 351–362.
- [34] LIU K J, WAN T Y, SHIBAYAMA A, MIYAZAK T, FUJITA T. Gold extraction from thiosulfate solution using trioctylmethylammonium chloride [J]. Hydrometallurgy, 2004, 73: 41–53.
- [35] ZENG Shi-lin, JIA Fei-fei, YANG Bing-qiao, SONG Shao-xian. In-situ reduction of gold thiosulfate complex on molybdenum disulfide nanosheets for a highly-efficient recovery of gold from thiosulfate solutions [J]. Hydrometallurgy, 2020, 195: 105369.
- [36] WANG Chao-wu, CHEN Shu-liang, CHEN Yun-long, ZI Fu-ting, HU Xian-zhi, QIN Xue-cong, ZHANG Yan, YANG Peng, HE Yi, HE Pu-qiang, LIN Yue, ZHANG Gui-fen. Modification of activated carbon by chemical vapour deposition through thermal decomposition of thiourea for enhanced adsorption of gold thiosulfate complex [J]. Separation and Purification Technology, 2020, 241: 116632.
- [37] FOTOOHI B, MERCIER L. Recovery of precious metals from ammoniacal thiosulfate solutions by hybrid mesoporous silica: 1—Factors affecting gold adsorption [J]. Separation and Purification Technology, 2014, 127: 84–96.
- [38] LU Tian, CHEN Fei-wu. Multiwfn: A multifunctional wavefunction analyzer [J]. Journal of computational

- chemistry, 2012, 33: 580–592.
- [39] WU Bai-le, WAN Jun, ZHANG Yan-yang, PAN Bing-cai, LO I M C. Selective phosphate removal from water and wastewater using sorption: Process fundamentals and removal mechanisms [J]. Environmental Science & Technology, 2020, 54: 50-66.
- [40] TRABOULSI A, DUPUY N, REBUFA C, SERGENT M, LABED V. Investigation of gamma radiation effect on the anion exchange resin Amberlite IRA-400 in hydroxide form by Fourier transformed infrared and ¹³C nuclear magnetic resonance spectroscopies [J]. Analytica Chimica Acta, 2012, 717: 110–121.
- [41] XU Bin, WU Jin-tian, DONG Zhong-lin, JIANG Tao, LI Qian, YANG Yong-bin. Flotation performance, structureactivity relationship and adsorption mechanism of a newlysynthesized collector for copper sulfide minerals in Gacun polymetallic ore [J]. Applied Surface Science, 2021, 551: 149420.
- [42] DONG Zhong-lin, JIANG Tao, XU Bin, LI Qian, ZHONG Hong, YANG Yong-bin. Selective flotation of galena using a novel collector S-benzyl-N-ethoxycarbonyl thiocarbamate: An experimental and theoretical investigation [J]. Journal of Molecular Liquids, 2021, 330: 115643.
- [43] DONG Zhong-lin, JIANG Tao, XU Bin, ZHONG Hong, ZHANG Bang-sheng, LIU Gui-qing, LI Qian, YANG Yong-bin. Density functional theory study on electronic structure of tetrahedrite and effect of natural impurities on its flotation property [J]. Minerals Engineering, 2021, 272: 106980.
- [44] XING Peng, MA Bao-zhong, WANG Cheng-yan, WANG Ling, CHEN Yong-qiang. A simple and effective process for recycling zinc-rich paint residue [J]. Waste Management, 2018, 76: 234–241.
- [45] WU Chong-chong, VISSCHER A D, GATES I D. Molecular interactions between 1-butyl-3-methylimidazolium tetra-fluoroborate and model naphthenic acids: A DFT study [J]. Journal of Molecular Liquids, 2017, 243: 462–471.

采用离子交换树脂从硫代硫酸盐溶液回收金的吸附行为和机理

董中林, 姜涛, 徐斌, 李骞, 杨永斌

中南大学 资源加工与生物工程学院,长沙 410083

摘 要:系统研究了硫代硫酸盐溶液中的金在强碱阴离子交换树脂上的吸附行为和机理。对金的吸附能力和选择性对比实验表明,具有 I 型季铵官能团的凝胶型 Amberlite IRA-400 树脂具有更好的吸附性能。树脂用量、氨浓度和溶液 pH 的增加有利于金的吸附,而二价铜离子和硫代硫酸盐浓度的增加不利于金的吸附。微观表征结果表明,金是通过与树脂官能团上的反离子 Cl-交换,以 $[Au(S_2O_3)_2]^3$ -配合物阴离子的形式被吸附。密度泛函理论计算结果表明,树脂对金的吸附主要依靠 $[Au(S_2O_3)_2]^3$ -中的 O 原子与树脂的季铵基官能团上的 H 原子之间形成的氢键和范德华力来实现。

关键词: 金; 硫代硫酸盐溶液; 树脂吸附; 行为和机理; 密度泛函理论计算